ADVANCED ELECTRONIC MATERIALS
www.advelectronicmat.de

Fluorinated Graphene Contacts and Passivation Layer for MoS_2 Field Effect Transistors

Huije Ryu, Dong-Hyun Kim, Junyoung Kwon, Sang Kyu Park, Wanggon Lee, Hyungtak Seo, Kenji Watanabe, Takashi Taniguchi, SunPhil Kim, Arend M. van der Zande, Jangyup Son, and Gwan-Hyoung Lee**

Realizing a future of 2D semiconductor-based devices requires new approaches to channel passivation and nondestructive contact engineering. Here, a facile one-step technique is shown that simultaneously utilizes monolayer fluorinated graphene (FG) as the passivation layer and contact buffer layer to 2D semiconductor transistors. Monolayer graphene is transferred onto the MoS_2, followed by fluorination by XeF_2 gas exposure. Metal electrodes for source and drain are fabricated on top of FG-covered MoS_2 regions. The MoS_2 transistor is perfectly passivated by insulating FG layer and, in the contacts, FG layer also acts as an efficient charge injection layer, leading to the formation of Ohmic contacts and high carrier mobility of up to 64 $cm^2 V^{-1} s^{-1}$ at room temperature. This work shows a novel strategy for simultaneous fabrication of passivation layer and low-resistance contacts by using ultrathin functionalized graphene, which has applications for high performance 2D semiconductor integrated electronics.

1. Introduction

2D materials have been considered as promising candidates for next-generation electronics since they offer unprecedented capability in device performance at the atomic limit through synergistic combination with silicon technology.[1,2] In particular, atomically thin 2D semiconductors, such as transition metal dichalcogenides (TMDs), have a desirable range of bandgap energies in the range between 1.0 and 2.5 eV and high carrier mobility up to 200 $cm^2 V^{-1} s^{-1}$,[3–6] thereby allowing integration into the silicon platforms. However, there are two ubiquitous problems that 2D semiconductors share with all nanomaterial electronics: environmentally

H. Ryu, G.-H. Lee
Department of Materials Science and Engineering
Seoul National University
Seoul 08826, Korea
E-mail: gwanlee@snu.ac.kr

D.-H. Kim, S. K. Park, J. Son
Functional Composite Materials Research Center
Korea Institute of Science and Technology (KIST)
Jeonbuk 55324, Korea
E-mail: jayson@kist.re.kr

D.-H. Kim
SKKU Advanced Institute of Nanotechnology (SAINT)
Sungkyunkwan University
Suwon 16419, Korea

J. Kwon
Department of Materials Science and Engineering
Yonsei University
Seoul 03722, Korea

W. Lee, H. Seo
Department of Materials Science and Engineering
Ajou University
Gyeonggi-do 16499, Korea

The ORCID identification number(s) for the author(s) of this article can be found under https://doi.org/10.1002/aelm.202101370.

DOI: 10.1002/aelm.202101370

K. Watanabe
Research Center for Functional Materials
National Institute for Materials Science
1-1 Namiki, Tsukuba 305-0044, Japan

T. Taniguchi
International Center for Materials Nanoarchitectonics
National Institute for Materials Science
1-1 Namiki, Tsukuba 305-0044, Japan

S. Kim, A. M. van der Zande
Department of Mechanical Science and Engineering
University of Illinois Urbana-Champaign (UIUC)
Urbana, IL 61801, USA

J. Son
Division of Nano and Information Technology
KIST School University of Science and Technology (UST)
Jeonbuk 55324, Korea

G.-H. Lee
Research Institute of Advanced Materials (RIAM)
Seoul National University
Seoul 08826, Korea

G.-H. Lee
Institute of Engineering Research
Seoul National University
Seoul 08826, Korea

G.-H. Lee
Institute of Applied Physics
Seoul National University
Seoul 08826, Korea

induced heterogeneity and contact engineering. First, environmental heterogeneity in the channel degrades device performance and leads to variability.[7,8] Second, traditional metallization induces structural disorder at the contact due to the high kinetic energy of evaporated metal source,[3] which results in the Fermi-level pinning and inevitable Schottky barriers at metal-2D semiconductor interfaces.[3,9,10] Realizing a future of 2D semiconductor-based devices requires new approaches to channel passivation and nondestructive contact engineering.

Graphene is an excellent electrical contact material for 2D semiconductors because it provides an atomically sharp and clean van der Waals gap, which reduces Fermi-level pinning and electrostatic work function modulation at the contact by electrostatic doping.[11–13] In particular, the chemical inertness and impermeability of graphene[14–16] make it an excellent metallization buffer layer to prevent degradation at the contacts.[17,18] However, passivating the semiconductor channel requires a material with resistance compared with the channel material. Thus, the high electrical conductivity of pristine graphene makes it impossible to use as the passivation layer.

Here, we demonstrated a novel fabrication process for MoS_2 field-effect transistors (FETs) using monolayer fluorinated graphene (FG) to act simultaneously as both the metallization buffer layer that plays the role of tunnel contacts and the passivation layer for MoS_2 channel. We fabricated a MoS_2 channel device passivated with monolayer graphene and exposed the XeF_2 gas to fluorinate the graphene layer. The interface between FG and MoS_2 is clean since there is no chance for 2D materials to be exposed to polymers or liquids during fabrication, yet, the FG layer prevents structural damages on the electrical contact area of MoS_2 from the metal atom bombardment during the metallization process. The FG passivation layer not only allows tunneling of the electrons from the contacts into the MoS_2 channel, but also protects the MoS_2 against contamination or chemical degradation. The FET showed excellent performance with Ohmic contacts, high on/off ration of 10^5, and high carrier mobility of 64 $cm^2\ V^{-1}\ s^{-1}$ at room temperature.

2. Results and Discussion

Figure 1 shows the fabrication process of the FG-passivated MoS_2 field-effect transistors (FG-MoS_2 FETs). Mechanically exfoliated monolayer graphene and monolayer MoS_2 on SiO_2/Si substrates were lifted sequentially by top hBN via pick-up technique (Figure S1, Supporting Information),[19] and top hBN/graphene/MoS_2 heterostructure was transferred onto the bottom hBN. Through e-beam lithography, the regions for electrical contacts were patterned on e-beam resist (ER) layer. Then, exposed hBN was etched away via XeF_2 gas treatment, and embedded graphene surface was fluorinated.[20] After the metal deposition and lift-off process, metal electrodes for the source and drain in the device were fabricated. Finally, through the second XeF_2 gas treatment, top hBN was etched and graphene was fluorinated. Through the technique described, we fabricated the final device as denoted with yellow-dashed box. Unlike the conventional fabrication methods, our fabrication strategy is facile since the device having both FG contacts and the electrical passivation layer is possible to be fabricated with only the transfer of monolayer graphene onto MoS_2 and the fluorination of graphene via XeF_2 gas treatment. Another remarkable advantage is that FG buffer layer prevents damage to MoS_2 during metallization to fabricate electrical contacts. In addition, there are no chances for graphene and MoS_2 to be exposed to polymers or liquid solvents during the whole fabrication process, thereby it is possible to fabricate devices with a clean surface/interface.

Figure 2a,b shows schematic illustrations and optical images of the device architecture before and after the final XeF_2 exposure

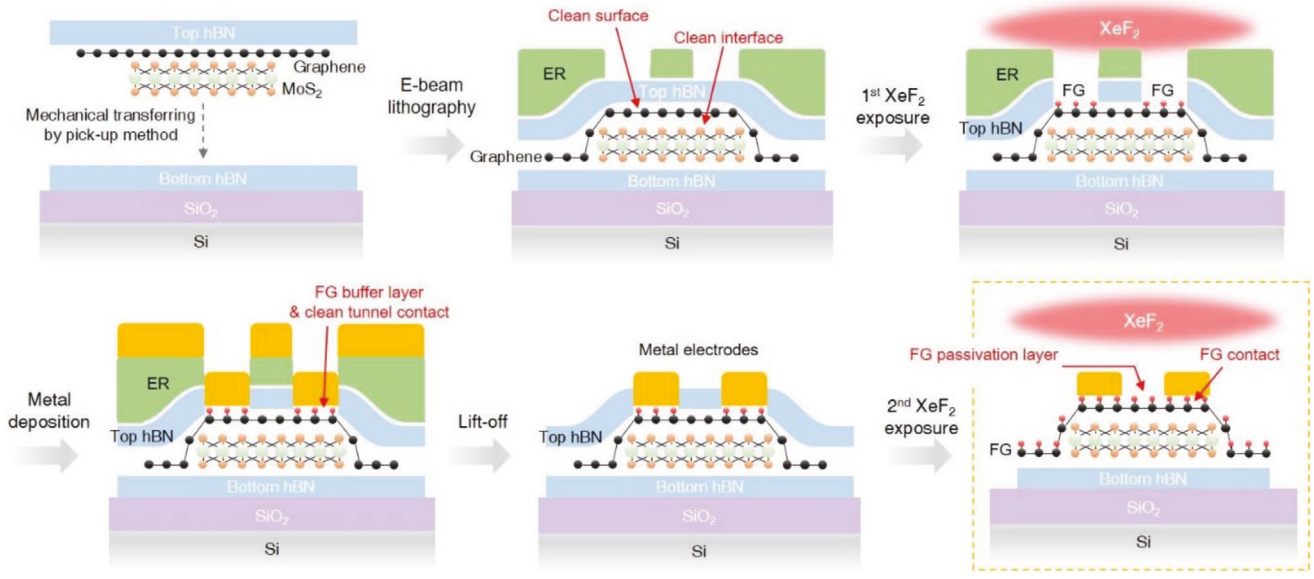

Figure 1. Schematic illustrations describing the fabrication process for the FG-passivated MoS_2 FET (FG-MoS_2 FET). The yellow dashed line indicates the final configuration of FG-MoS_2 FET incorporating both the FG-tunnel contact buffer layer and the FG-passivation layer.

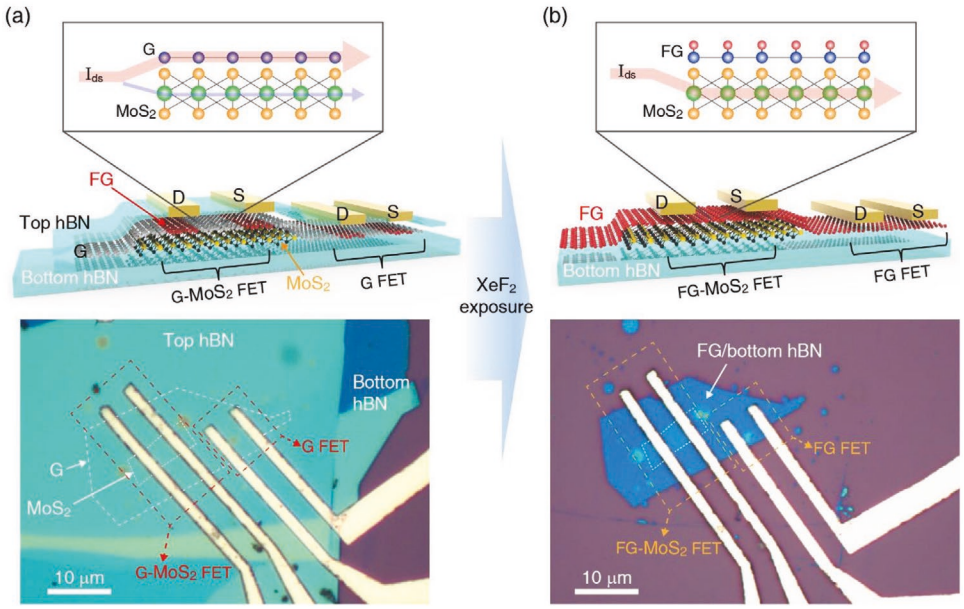

Figure 2. Schematic illustrations and optical images of graphene-passivated MoS_2 FET (G-MoS_2 FET) and graphene FET (G FET) a) before and b) after XeF_2 gas exposure. The electrical current flows along the conductive graphene channel (a) before XeF_2 gas treatment, while the current flows along the MoS_2 channel (b) after the fluorination of graphene layer.

respectively. Clearly visible in the optical images between Figure 2a,b, as a result of the XeF_2 exposure, the top hBN layer on the graphene was completely etched. The embedded graphene acts as an etch stop, so any regions under the graphene remain unetched.[16] Before exposure, the graphene in the channel is pristine, so the device acts as a G-MoS_2 heterostructure. After exposure, the channel consists of FG-MoS_2. In addition, to independently confirm the effect of fluorination on the graphene, we also fabricated a graphene FET without MoS_2 on the same hBN, shown as G FET in Figure 2a and FG FET in Figure 2b. The inset boxes on Figure 2a,b show the change in the mechanism of transport. Before exposure, most of the electrical current flows through the pristine graphene due to the lower resistance of the graphene than that of the MoS_2. In contrast, when the overlying graphene was fluorinated, the underlying MoS_2 was maintained without any damage due to the etching stop function of FG,[16] and the electrical current passes through MoS_2 channel.[20,21] Taken together, we note that FG is used as both the contact buffer layer and electrical passivation layer for MoS_2 at the same time.

Figure 3 shows the changes in the structure and optical properties of the Gr/MoS_2/hBN stack, with the Raman and photoluminescence (PL) spectra before and after XeF_2 gas exposure. Figure 3a shows the Raman spectra of Gr/MoS_2/hBN stack before and after fluorination. Before fluorination, the A_{1g} vibrational mode of MoS_2 is maintained, meanwhile the E^1_{2g} vibrational mode of that shows slight blue-shift after fluorination. This indicates that the MoS_2 is protected from XeF_2 except for formation of slight compressive strain due to the structural deformation of the FG.[22,23] Before fluorination, Raman data shows the G (1582 cm^{-1}), 2D (2696 cm^{-1}) vibrational modes of graphene, and Raman peak of hBN (1366 cm^{-1}), which are

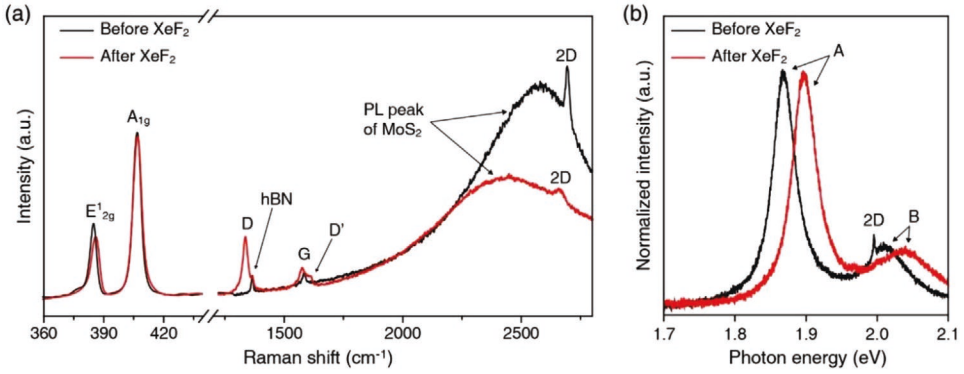

Figure 3. Raman and photoluminescence spectra of FG-passivated MoS_2. a) Raman spectra of Gr/MoS2/hBN stack before and after fluorination. Background signal is resulted from the PL peak of MoS_2. The decrease of 2D Raman peak and increase of D and D′ Raman peak indicates the formation of sp^3 bonds onto the graphene surface after fluorination. b) Normalized photoluminescence spectra of MoS_2 under graphene before and after fluorination.

generally observed in graphene/hBN heterostructure. The broad peak around 2400 cm^{-1} is PL peak of the MoS_2. After fluorination, as reported in the previous study on fluorination of graphene via XeF_2 gas treatment,[20] the D (1336 cm^{-1}) and D′ (1614 cm^{-1}) vibrational modes emerged, and the G and 2D peaks were suppressed. As generally studied, defects in graphene break the symmetry of the carbon honeycomb lattice and change carbon-hybridization from sp^2 into sp^3.[24] As a result, the G and 2D peaks that satisfy the Raman selection rule are suppressed and the Raman-forbidden D and D′ bands become stronger in the spectrum as the fluorination of graphene proceeds,[24–26] which is in agreement with our observation. Figure 3b shows the normalized PL spectra of MoS_2 before and after fluorination of overlying graphene. The PL peaks of A- and B-excitons in the MoS_2 blue-shifted by ≈30 meV after fluorination, which results from the change of dielectric screening and compressive strain from the fluorination of graphene.[23,27] As the electrical property of graphene changes from metal to insulator by fluorination, the Coulomb interactions in electron–hole pairs of MoS_2 increase with decreasing the dielectric screening effect, which increases the bandgap of MoS_2.[28] As a result, the photon energy of maximum PL intensity in MoS_2 shows right-shift after fluorination of graphene. Most importantly, we note that the FWHM of A-exciton peak is almost constant at about 40 meV, before and after exposure, indicating that the graphene fluorination process does not induce the severe damage in MoS_2.

Figure 4 compares the electrical transport measurements of the G/MoS_2/hBN and FG/MoS_2/hBN FETs. We used the degenerately doped Si substrate as a global back gate, while the hBN/SiO_2 acted as the gate dielectric. Figure 4a plots the transfer curves of the G FET (red curve) and G-MoS_2 FET (blue curve) shown in Figure 2a before XeF_2 exposure. Both the GFET and G-MoS_2 FET showed the characteristic graphene transport curve. Compared to the G FET, the G-MoS_2 FET showed increased current, i.e., lower resistance, and charge neutrality point (CNP) shifted to zero voltage. This shows that the current mainly flows through the graphene.[29]

After measurements, the two FETs were exposed to XeF_2 gas to transform into FG/hBN (FG FET) and FG/MoS_2/hBN (FG-MoS_2 FET) as discussed in Figure 2b. Figure 4b plots the transfer curves of FG FET (red curve) and FG-MoS_2 FET (blue curve). The FG FET showed a low current 10^{-11} A with no gate dependence, indicating that the FG is completely insulating as reported before.[16] The FG-MoS_2 FET showed a typical n-type FET gate dependence, similar to MoS_2 devices.[15,16] This means that the underlying MoS_2 is perfectly passivated by the FG during fluorination.[20,21] Moreover, the FG-MoS_2 FET showed a high field-effect mobility of 64 cm^2 V^{-1} s^{-1} with on/off current ratio of 10^5 (we confirmed the reproducible performance with three more FETs as shown in Figure S2 in the Supporting Information). As shown in Figure 4c, the output curves (V_{ds}–I_{ds}) of the FG-MoS_2 FET showed a linear behavior over a broad range in gates, which is indicative of the Ohmic contact at Cr/FG/MoS_2 interface. The improved performance of the devices is attributed to low contact resistance and FG-passivation of MoS_2, that prevents exposure of MoS_2 to any polymers or liquid solutions during fabrication process. We hypothesize that the FG layer in the contact regions protects the MoS_2 from metal atom bombardment during metallization, leading to enhancement of contact properties by reducing the Fermi level pinning between metal and MoS_2.[2,18] Moreover, the insulating FG layer is operated as a tunnel barrier for electrons and reduces the metal-induced gap states in MoS_2, which reduces the Schottky barrier height (see Figure S3 in the Supporting Information).[30,31] As a result, FG-inserted metal-MoS_2 contact shows the Ohmic contact with low contact resistance.

As hydrogenation is another way to open the bandgap of graphene as wide as 4.0 eV,[32,33] we modified the process to also fabricated another FET where MoS_2 channel is electrically passivated with hydrogenated graphene (HG) to form the HG-MoS_2 FET (process and image in Figure S4 in the Supporting Information). **Figure 5** shows the transport data in the G-MoS_2 FET (red curve) and HG-MoS_2 FET (blue curve) before and after hydrogenation respectively. Before hydrogenation of graphene, the G-MoS_2 FET showed the field effect behavior observing in p-doped graphene, indicating the electrical current flows along through graphene. After hydrogenation of graphene via indirect hydrogen plasma for 1000 s, the HG-MoS_2 FET showed field-effect behavior similar to in n-type MoS_2, just as was observed in the FG-MoS_2 FET in Figure 4b, indicating, that the electrical current flows through the MoS_2 channel under the electrically insulating HG layer. However, unlike FG-MoS_2 FET, HG-MoS_2

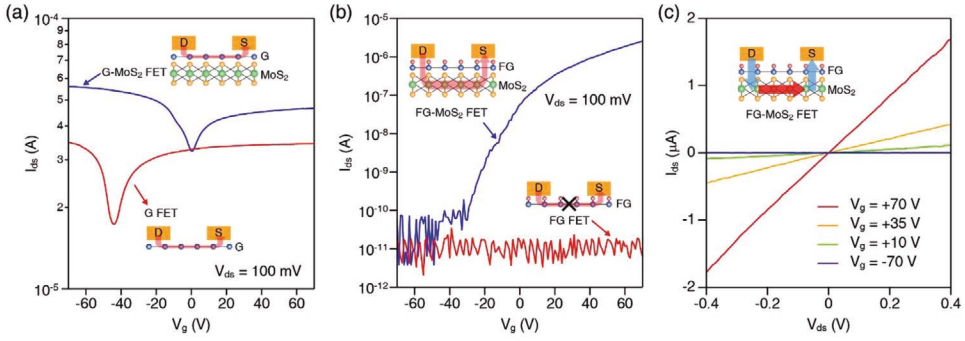

Figure 4. Electrical properties of hBN/Gr/MoS_2/hBN (G-MoS_2 FET) and hBN/Gr/hBN (G FET) structures before and after fluorination process. a) V_g–I_{ds} characteristics for G-MoS_2 FET and G FET structures before XeF_2 gas exposure. b) V_g–I_{ds} characteristics for FG/MoS_2/hBN (FG-MoS_2 FET) and FG/hBN (FG FET) structures. The n-type operation of FG-MoS_2 FET results from transconductance change of MoS_2, which means almost electrical current passes through MoS_2 layer since graphene becomes insulator after fluorination via XeF_2 gas exposure. c) V_{ds}–I_{ds} curves for FG-MoS_2 FET. Linear behavior indicates Ohmic contact between metal electrodes and MoS_2.

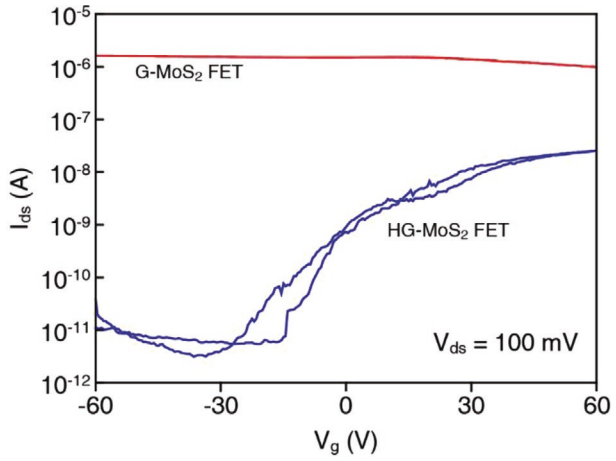

Figure 5. The changes in FET characteristic of G-MoS_2 FET before and after hydrogenation. To electrically passivate conducting graphene in graphene/MoS_2 heterostructure, we hydrogenated top graphene by low-energy indirect hydrogen plasma for 1000 s. HG-MoS_2 FET showed a change in current of over 10^3 on/off ratio. However, ON current level also decrease after hydrogenation. Although graphene was mildly hydrogenated by indirect hydrogen plasma, it is assumed that inevitable defects are generated during hydrogenation of graphene via plasma treatment.

FET showed a relatively low field-effect mobility of 2 $cm^2\ V^{-1}\ s^{-1}$ with on/off current ratio of 10^3. We hypothesize that, unlike the gas phase fluorination of graphene via XeF_2, the indirect hydrogen plasma used for hydrogenation of graphene generates damages the MoS_2 under graphene (Figure S5, Supporting Information) or electrical contact regions due to the transferring of ion energy. On the basis of the results, we recommend that the fluorination of top graphene on MoS_2 channel via XeF_2 gas treatment is the more proper and nondestructive approach to fabricate the functionalized-graphene-passivated MoS_2 devices with high electrical properties.

3. Conclusion

In conclusion, we report the facile fabrication way to incorporate both tunneling contact buffer layer and passivation layer to MoS_2 FETs via the fluorination of monolayer graphene encapsulating MoS_2 channel. Contrary to the conventional fabrication processes using elaborate transfer technique that aligns graphene to the electrical contact area on MoS_2 and complicated patterning, our work reveals that FG-passivated MoS_2 FETs incorporating both tunneling contacts and passivation layer may be fabricated only with graphene transfer and fluorination. Moreover, the devices with a clean surface/interface are fabricated since graphene and MoS_2 are not exposed to polymers and liquid solutions during all processes. Graphene-passivated MoS_2 FETs fabricated by the technique show Ohmic contact behavior, on/off ratio of 10^5, and the carrier mobility of up to 64 $cm^2\ V^{-1}\ s^{-1}$ after the fluorination of graphene layer, supporting that our strategy is suitable for devices with high electrical performance. This work is compatible with conventional 2D semiconductor processes and provides a facile way for the fabrication of 2D semiconductor-based devices.

4. Experimental Section

Fabrication of FG Contacts and Electrical/Surface Passivation Layer for MoS_2 FETs: All 2D flakes used in this work were mechanically exfoliated onto SiO_2/Si substrates by the Scotch tape method. Thicknesses of the exfoliated graphene and MoS_2 were measured using the Raman spectroscopy (Figure S1, Supporting Information). An exfoliated monolayer graphene was transferred onto a monolayer MoS_2 using the pick-up transfer technique.[19]

As shown in Figure 1, a stack of hBN/MoS_2/Gr/hBN was prepared, then carried out e-beam lithography to pattern metal electrodes. The hBN in the patterned regions was etched away by XeF_2 exposure (Xactix etching system, P_{XeF_2} = 3 Torr, t = 2 min). In general, the exposure time for etching depends on the thickness of hBN, thereby it could be set according to the thickness of the top layer of hBN. For ≈40-nm-thick hBN, the exposure time for etching was about 1 min;[16,20] therefore, hBN to XeF_2 gas was exposed for 2 min to completely etch. After etching of top hBN, the embedded graphene layer was fluorinated, preventing further etching as reported previously.[16] Then, metals of Cr/Pd/Au (1 nm/30 nm/40 nm) were deposited on the FG regions using an e-beam evaporator (KVE-E2000L, Korea Vacuum Tech.). The lift-off process was performed by soaking the sample in acetone. To change the graphene on the MoS_2 to the insulating passivation layer, the remaining hBN was etched and graphene was simultaneously fluorinated by a second XeF_2 exposure (P_{XeF_2} = 3 Torr, t = 12 min). As graphene turns into fluorinated graphene (FG), the electrical conductivity decreases with increasing XeF_2 exposure time,[16,20] achieving insulating behavior at 10 min. Therefore, the heterostructure was overexposed to the XeF_2 gas for 12 min to both etch the hBN and fluorinate the graphene.

Raman Spectroscopy and Photoluminescence (PL) Measurements: The Raman PL spectra were measured by Raman spectroscopy (Renishaw) with a laser of 532 nm. To minimize the damage of the samples by the laser irradiation, Raman signals were obtained with a small power of 47 $\mu W\ \mu m^{-2}$ for an acquisition time of 60 s.

Electrical Measurements: The electrical measurements of the MoS_2 FETs were conducted using a semiconductor parameter analyzer (Keithley 2400) under ambient conditions.

Supporting Information

Supporting Information is available from the Wiley Online Library or from the author.

Acknowledgements

H.R. and D.-H.K. contributed equally to this work. This work was supported by the National Research Foundation of Korea (NRF-2021R1A2C3014316 and NRF-2018M3D1A1058793), the Creative-Pioneering Researchers Program through Seoul National University (SNU), the National Research Council of Science & Technology (NST) grant by the Korea government (MSIT) (No. CRC-20-01-NFRI), the National Research Foundation of Korea (NRF) funded by the Ministry of Science and ICT (NRF-2021M3H4A1A01079358), and the National Science Foundation MRSEC program under NSF Award Number DMR-1720633. This work was carried out in the Material Research Laboratory Central Facilities, the Micro and Nano Technology Laboratory, and the iMRSEC shared facilities DMR-1720633.

Conflict of Interest

The authors declare no conflict of interest.

Data Availability Statement

Research data are not shared.

Keywords

2D materials heterostructure, electrical passivation, fluorination, graphene, MoS_2

Received: December 17, 2021
Revised: February 23, 2022
Published online:

[1] D. Akinwande, C. Huyghebaert, C.-H. Wang, M. I. Serna, S. Goossens, L.-J. Li, H.-S. P. Wong, F. H. L. Koppens, *Nature* **2019**, *573*, 507.
[2] C. Liu, H. Chen, S. Wang, Q. Liu, Y.-G. Jiang, D. W. Zhang, M. Liu, P. Zhou, *Nat. Nanotechnol.* **2020**, *15*, 545.
[3] Y. Liu, J. Guo, E. Zhu, L. Liao, S.-J. Lee, M. Ding, I. Shakir, V. Gambin, Y. Huang, X. Duan, *Nature* **2018**, *557*, 696.
[4] S.-L. Li, K. Komatsu, S. Nakaharai, Y.-F. Lin, M. Yamamoto, X. Duan, K. Tsukagoshi, *ACS Nano* **2014**, *8*, 12836.
[5] Y. Wang, J. C. Kim, R. J. Wu, J. Martinez, X. Song, J. Yang, F. Zhao, A. Mkhoyan, H. Y. Jeong, M. Chhowalla, *Nature* **2019**, *568*, 70.
[6] F. Xia, H. Wang, D. Xiao, M. Dubey, A. Ramasubramaniam, *Nat. Photonics* **2014**, *8*, 899.
[7] A. Raja, A. Chaves, J. Yu, G. Arefe, H. M. Hill, A. F. Rigosi, T. C. Berkelbach, P. Nagler, C. Schüller, T. Korn, C. Nuckolls, J. Hone, L. E. Brus, T. F. Heinz, D. R. Reichman, A. Chernikov, *Nat. Commun.* **2017**, *8*, 15251.
[8] A. Raja, L. Waldecher, J. Zipfel, Y. Cho, S. Brem, J. D. Ziegler, M. Kulig, T. Taniguchi, K. Watanabe, E. Malic, T. F. Heinz, T. C. Berkelbach, A. Chernikov, *Nat. Nanotechnol.* **2019**, *4*, 832.
[9] W. A. Saidi, *J. Chem. Phys.* **2014**, *141*, 094707.
[10] J. Kang, W. Liu, D. Sarkar, D. Jena, K. Banerjee, *Phys. Rev. X* **2014**, *4*, 031005.
[11] Y. Liu, H. Wu, H.-C. Cheng, S. Yang, E. Zhu, Q. He, M. Ding, D. Li, J. Guo, N. O. Weiss, Y. Huang, X. Duan, *Nano Lett.* **2015**, *15*, 3030.
[12] Y. T. Lee, K. Choi, H. S. Lee, S.-W. Min, P. J. Jeon, D. K. Hwang, H. J. Choi, S. Im, *Small* **2014**, *10*, 2356.
[13] L. Yu, Y.-H. Lee, X. Ling, E. J. G. Santos, Y. C. Shin, Y. Lin, M. Dubey, E. Kaxiras, J. Kong, H. Wang, T. Palacios, *Nano Lett.* **2014**, *14*, 3055.
[14] G.-H. Lee, R. C. Cooper, S. J. An, S. Lee, A. van der Zande, N. Petrone, A. G. Hammerberg, C. Lee, B. Crawford, W. Oliver, J. W. Kysar, J. Hone, *Science* **2013**, *340*, 1073,.
[15] J. S. Bunch, S. S. Verbridge, J. S. Alden, A. M. van der Zande, J. M. Parpia, H. G. Craighead, P. L. McEuen, *Nano Lett.* **2008**, *8*, 2458.
[16] J. Son, J. Kwon, S. Kim, Y. Lv, J. Yu, J.-Y. Lee, H. Ryu, K. Watanabe, T. Taniguchi, R. Garrido-Menacho, N. Mason, E. Ertekin, P. Y. Huang, G.-H. Lee, A. M. van der Zande, *Nat. Commun.* **2018**, *9*, 3988.
[17] S.-S. Chee, D. Seo, H. Kim, H. Jang, S. Lee, S. P. Moon, K. H. Lee, S. W. Kim, H. Choi, M.-H.o Ham, *Adv. Mater.* **2019**, *31*, 1804422.
[18] R. Zan, Q. M. Ramasse, R. Jalil, T. Georgiou, U. Bangert, K. S. Novoselov, *ACS Nano* **2013**, *7*, 10167.
[19] F. Pizzocchero, L. Gammelgaard, B. S. Jessen, J. M. Caridad, L. Wang, J. Hone, P. Boggild, T. J. Booth, *Nat. Commun.* **2016**, *7*, 11894.
[20] J. T. Robinson, J. S. Burgess, C. E. Junkermeier, S. C. Badescu, T. L. Reinecke, F. K. Perkins, M. K. Zalalutdniov, J. W. Baldwin, J. C. Culbertson, P. E. Sheehan, E. S. Snow, *Nano Lett.* **2010**, *10*, 3001.
[21] R. R. Nair, W. Ren, R. Jalil, I. Riaz, V. G. Kravets, L. Britnell, P. Blake, F. Schedin, A. S. Mayorov, S. Yuan, M. I. Katsnelson, H.-M. Cheng, W. Strupinski, L. G. Bulusheva, A. V. Okotrub, I. V. Grigorieva, A. N. Grigorenko, K. S. Novoselov, A. K. Geim, *Small* **2010**, *6*, 2877.
[22] R. J. Kashtiban, M. A. Dyson, R. R. Nair, R. Zan, S. L. Wong, Q. Ramasse, A. K. Geim, U. Bangert, J. Sloan, *Nat. Commun.* **2014**, *5*, 4902.
[23] S. Pak, J. Lee, Y.-W. Lee, A.-R. Jang, S. Ahn, K. Y. Ma, Y. Cho, J. Hong, S. Lee, H. Y. Jeong, H. Im, H. S. Shin, S. M. Morris, S. Cha, J. I. Sohn, J. M. Kim, *Nano Lett.* **2017**, *17*, 5634.
[24] A. Eckmann, A. Felten, A. Mishchenko, L. Britnell, R. Krupke, K. S. Novoselov, C. Casiraghi, *Nano Lett.* **2012**, *12*, 3925.
[25] F. Tuinstra, J. Koenig, *J. Chem. Phys.* **1970**, *53*, 1126.
[26] A. C. Ferrari, *Solid State Commun.* **2007**, *143*, 47.
[27] E. Lorchat, L. E. P. Lopez, C. Robert, D. Lagarde, G. Froehlicher, T. Taniguchi, K. Watanabe, X. Marie, S. Berciaud, *Nat. Nanotechnol.* **2020**, *15*, 283.
[28] A. Chernikov, T. C. Berkelbach, H. M. Hill, A. Rigosi, Y. Li, O. B. Aslan, D. R. Reichman, M. S. Hybertsen, T. F. Heinz, *Phys. Rev. Lett.* **2014**, *113*, 076802.
[29] C. R. Dean, A. F. Young, I. Meric, C. Lee, L. Wang, S. Sorgenfrei, K. Watanabe, T. Taniguchi, P. Kim, K. L. Shepard, J. Hone, *Nat. Nanotechnol.* **2010**, *5*, 722.
[30] X.-X. Li, Z.-Q. Fan, P.-Z. Liu, M.-L. Chen, X. Liu, C.-K. Jia, D.-M. Sun, X.-W. Jiang, Z. Han, V. Bouchiat, J.-J. Guo, J.-H. Chen, Z.-D. Zhang, *Nat. Commun.* **2017**, *8*, 6842.
[31] J. Wang, Q. Yao, C.-W. Huang, X. Zou, L. Liao, S. Chen, Z. Fan, K. Zhang, W. Wu, X. Xiao, C. Jiang, W.-W. Wu, *Adv. Mater.* **2016**, *28*, 8302.
[32] H. Gao, L. Wang, J. Zhao, F. Ding, J. Lu, *J. Phys. Chem. C* **2011**, *115*, 3236.
[33] J. Son, S. Lee, S. J. Kim, B. C. Park, H.-K. Lee, S. Kim, J. H. Kim, B. H. Hong, J. Hong, *Nat. Commun.* **2016**, *7*, 1326.